Journal of the Korean Crystal Growth and Crystal Technology
Vol. 35, No. 3 (2025) 105-110
https://doi.org/10.6111/JKCGCT.2025.35.3.105

p-ISSN 1225-1429
e-ISSN 2234-5078

Hydrothermal synthesis of nickel selenides on Ni foam for electrocatalytic oxygen evolution

Tae Kwang An, Yun Seok Jang, Dong Hyun You, Hyun Cho*,† and Jeong Ho Ryu†

Department of Materials Science and Engineering, Korea National University of Transportation, Chungju 27469, Korea
**Department of Nanomechatronics Engineering, Pusan National University, Busan 46241, Korea*

(Received September 8, 2025)
(Revised September 10, 2025)
(Accepted September 10, 2025)

Abstract Nickel selenides have emerged as promising electrocatalysts for the oxygen evolution reaction (OER) due to their high conductivity, tunable electronic structure, and ability to transform into catalytically active oxyhydroxides under alkaline conditions. In this study, nickel selenides were directly synthesized on Ni foam via a simple hydrothermal process using elemental selenium powder and hydrazine as precursors. The synthesis temperature was systematically varied from 120 to 200°C to investigate its influence on phase formation, morphology, and electrocatalytic activity. Structural analysis by X-ray diffraction (XRD) revealed a gradual evolution from poorly crystallized products at low temperature to highly crystalline $NiSe_2$/Ni_3Se_2 phases at elevated temperature, with the NS-160 sample (160°C) exhibiting the most balanced crystalline structure. FE-SEM and EDS analyses confirmed that NS-160 possessed a uniform nanosheet-like morphology and a homogeneous Ni-Se distribution. Electrochemical evaluation demonstrated that NS-160 delivered the best OER performance, requiring the lowest overpotential (η_{100}) to achieve 100 $mA \cdot cm^{-2}$, the smallest Tafel slope, and the lowest charge-transfer resistance, along with the highest double-layer capacitance (C_{dl}) and electrochemically active surface area (ECSA). These results highlight that optimized crystallinity and morphology at 160°C yield superior electrocatalytic activity by maximizing accessible active sites and facilitating rapid charge transport. This work provides a cost-effective and scalable route for fabricating efficient nickel selenide-based electrodes for alkaline water electrolysis.

Key words Nickel selenides, Hydrothermal synthesis, Ni foam-supported catalysis, Oxygen evolution reaction (OER), Electrocatalysis

1. Introduction

The growing global demand for sustainable and renewable energy sources has placed electrochemical water splitting at the forefront of clean hydrogen production technologies. Among the two half-reactions, the oxygen evolution reaction (OER) is widely recognized as the kinetic bottleneck due to its sluggish four-electron transfer process and high overpotential requirements. To overcome these challenges, the development of efficient, durable, and cost-effective OER electrocatalysts has become a major research priority. Traditionally, noble metal-based catalysts such as IrO_2 and RuO_2 have demonstrated excellent catalytic activity toward OER [1-3]. However, their high cost, scarcity, and poor long-term stability in alkaline conditions severely limit their large-scale applications. Therefore, the exploration of earth-abundant transition-metal-based compounds as alternative OER electrocatalysts has attracted increasing attention [4,5].

Among various transition-metal-based materials, nickel selenides have emerged as promising candidates for OER catalysis owing to their intrinsic electrical conductivity, rich redox chemistry, and favorable electronic structure. In particular, nickel selenides offer better charge transfer properties compared to their oxide or hydroxide counterparts, enabling faster electron transport during the OER process [6,7]. Moreover, the presence of selenium atoms can effectively modulate the electronic configuration of nickel, thereby enhancing the density of active sites and catalytic performance. Recent studies have reported that nickel selenide nanostructures, when combined with conductive substrates or doped with other transition metals, exhibit remarkable OER activity. However, many of these synthetic strategies involve complex procedures, expensive precursors, or require additional post-treatments, which hinder their scalability and practical deployment [8,9].

To address these limitations, we focus on a facile hydrothermal synthesis route using elemental selenium powder and hydrazine as precursors for nickel selenide

†Corresponding author
E-mail: hyuncho@pusan.ac.kr, jhryu@ut.ac.kr

formation. This approach not only reduces the cost of synthesis but also eliminates the need for sophisticated processing steps. Importantly, the direct growth of nickel selenides on conductive Ni foam provides a binder-free, self-supported electrode architecture, which facilitates efficient charge transfer, strong mechanical stability, and exposure of abundant electroactive sites. Such self-supported electrode structures are particularly advantageous for practical water electrolysis applications, as they circumvent the drawbacks associated with powder-based catalysts that require polymeric binders and conductive additives, which often hinder electron and ion transport [10].

In this study, we report the hydrothermal synthesis of nickel selenides on Ni foam using Se powder and hydrazine as precursors, followed by a systematic evaluation of their OER performance. The structural and morphological evolution of the nickel selenides at different synthesis conditions was characterized by X-ray diffraction (XRD) and field emission scanning electron microscopy (FE-SEM). The electrocatalytic performance was assessed via linear sweep voltammetry (LSV), Tafel slope analysis, and electrochemical impedance spectroscopy (EIS). Our findings demonstrate that the optimized nickel selenide/Ni foam electrode exhibits enhanced OER activity, low overpotential, and highlighting the potential of this simple and cost-effective synthesis strategy for scalable hydrogen production technologies.

2. Experimentals

Ni foam sheets were cut into 1.0 × 2.0 cm pieces (geometric area 2.0 cm^2). Each piece was ultrasonically cleaned in acetone, ethanol, and DI water for 10 min each to remove organics, followed by a brief acid etch in 1.0 M HCl for 10 min to eliminate native oxides. The foams were thoroughly rinsed with DI water and dried at 60°C. For mass loading determination, the dry mass of each Ni foam was recorded (m_0) to a precision of 0.01 mg. A Teflon-lined stainless-steel autoclave (50 mL) was used. In a typical synthesis, 20 mL of DI water containing hydrazine hydrate (volume fraction 5 vol%) was prepared as the reaction medium. Selenium powder (typically 10~20 mg per autoclave) was added and magnetically stirred for 10 min to obtain a well-dispersed suspension. A pre-treated Ni foam (Section above) was vertically immersed in the suspension using a PTFE holder to avoid contact with the vessel wall. The autoclave was sealed and heated to the target temperature T = 120, 140, 160, 180, or 200°C for 6 h, then allowed to cool naturally to room temperature. The resultant Ni foam supported nickel selenide electrodes were removed, rinsed sequentially with DI water and ethanol to remove residual ions/precursors, and dried at 60°C. Samples are denoted (a) NS-120, (b) NS-140, (c) NS-160, (d) NS-180, and (e) NS-200, corresponding to the hydrothermal treatment temperature.

X-ray diffraction (XRD). Powder XRD patterns of the as-grown electrodes (air-dried, without scraping) were recorded with Cu Kα radiation (λ = 1.5406 Å) at 40 kV and 40 mA over 2θ = 10~80°, step size 0.02°, and scan rate 2° min^{-1}. Phase identification was carried out by comparison with standard reference patterns (ICDD PDF). The intense reflections from the Ni foam substrate were used as internal references when applicable. Field-emission scanning electron microscopy (FE-SEM). Surface and cross-sectional morphologies were examined using FE-SEM at an accelerating voltage of 5~10 kV. Prior to imaging, samples were gently blown with nitrogen to remove loose particles. Elemental distributions were optionally probed by EDS mapping to confirm the presence and homogeneity of Ni and Se on the foam ligaments.

Electrochemical measurements were carried out in 1.0 M KOH using a three-electrode system with the nickel selenide/Ni foam electrode as the working electrode, a Pt mesh as the counter electrode, and an Ag/AgCl (3 M KCl) electrode as the reference. All potentials were converted to the reversible hydrogen electrode (RHE) scale. The as-prepared electrodes were directly used without additional binders. Linear sweep voltammetry (LSV) was conducted at a scan rate of 5 mV/s to evaluate OER activity, and the overpotential at 100 mA·cm^{-2} (η_{100}) was determined. Tafel slopes were derived from the LSV curves to analyze reaction kinetics. Electrochemical impedance spectroscopy (EIS) was performed in the frequency range of 100 kHz to 0.1 Hz at an overpotential of ~300 mV to estimate charge-transfer resistance. The double-layer capacitance (C_{dl}) was obtained from cyclic voltammetry in a non-faradaic region at scan rates from 10 to 100 mV/s, and the electrochemically active surface area (ECSA) was estimated accordingly [11].

3. Results and Discussion

Figure 1 shows the XRD patterns of the NS-120, NS-140, NS-160, NS-180, and NS-200 samples synthesized

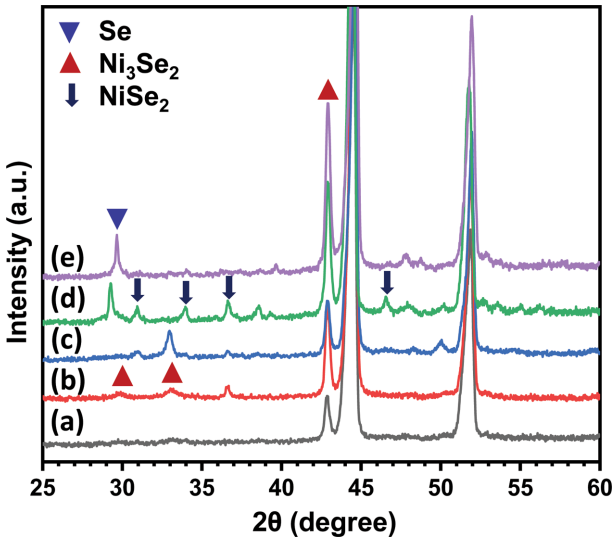

Fig. 1. XRD patterns of the of the (a) NS-120, (b) NS-140, (c) NS-160, (d) NS-180 and (e) NS-200 samples.

at different hydrothermal temperatures. Besides the characteristic reflections from Ni foam ($2\theta \approx 44.5^{o}$ and 51.8^{o}), additional peaks corresponding to nickel selenides are observed. At 120°C (NS-120), the diffraction peaks are weak and broad, indicating the presence of poorly crystallized phases. Only faint reflections near $2\theta \approx 31^{o}$ and 45^{o} can be discerned, suggesting incipient formation of Ni-Se compounds but incomplete selenization of the Ni substrate. When the temperature is raised to 140°C (NS-140), more distinct peaks appear at $2\theta \approx 29.5^{o}$, 33.5^{o}, and 45.2^{o}, which can be indexed to the (200), (210), and (211) planes of $NiSe_2$ (PDF# 41-1495). Additionally, reflections at $2\theta \approx 34.6^{o}$ and 37.9^{o} match the (202) and (113) planes of Ni_3Se_2 (PDF# 44-1418). This confirms partial transformation of nickel into crystalline selenides, although the relative intensities remain low, reflecting limited crystallinity.

At 160°C (NS-160), the diffraction peaks become sharper and more intense, with well-defined reflections at $2\theta \approx 29.5^{o}$, 33.5^{o}, 45.2^{o} ($NiSe_2$) and 34.6^{o}, 37.9^{o}, 49.7^{o} (Ni_3Se_2). The coexistence of $NiSe_2$ and Ni_3Se_2 phases with improved crystallinity suggests that this temperature provides optimal conditions for selenization, yielding a robust crystalline backbone with favorable electrical conductivity and catalytic potential. At higher temperatures (180 and 200°C; NS-180 and NS-200), the nickel selenide peaks further intensify, indicating continued crystal growth. However, in addition to the main $NiSe_2$/Ni_3Se_2 reflections, small features attributable to elemen-

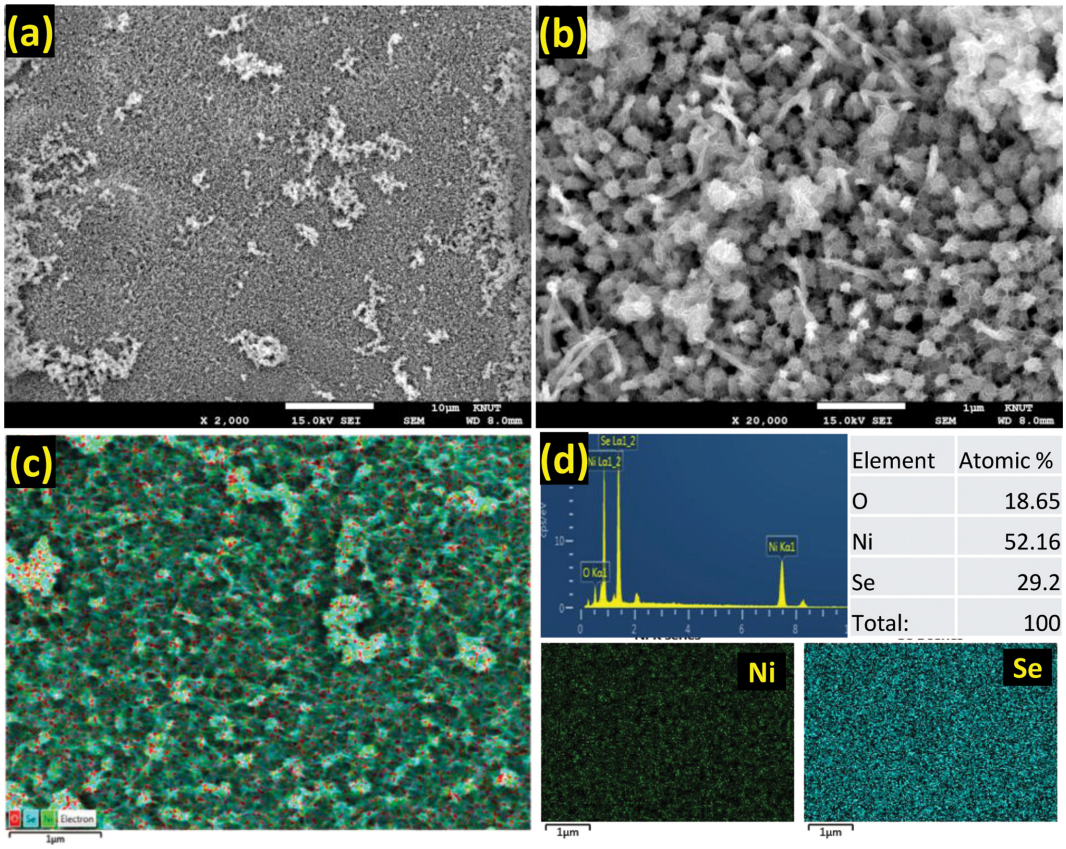

Fig. 2. FE-SEM images (a, b) and EDS data (c, d) of the NS-160 sample.

tal Se (e.g., $2\theta \approx 23.5^{\circ}$ and 29.8°) emerge, implying that at elevated temperatures excess selenium may recrystallize or deposit on the Ni foam surface. This can lead to thicker layers or inhomogeneous coverage, potentially impeding charge and mass transfer during electrocatalysis.

The surface morphology of the optimized NS-160 sample was examined by FE-SEM, and the results are presented in Fig. 2. At low magnification (Fig. 2a), the Ni foam substrate is uniformly coated with a continuous layer of nickel selenides, confirming that hydrothermal treatment at 160°C leads to homogeneous deposition over the entire 3D porous framework. No bare regions of Ni foam are visible, indicating effective surface coverage. The higher-magnification image (Fig. 2b) reveals that the deposited nickel selenides form interconnected nanosheet and nanoparticle-like features. Such hierarchical structures increase the surface roughness and porosity, thereby enhancing electrolyte penetration and facilitating exposure of electrochemically active sites. Elemental composition was confirmed by EDS analysis. The mapping images (Fig. 2c) show that Ni and Se elements are homogeneously distributed throughout the foam ligaments, demonstrating that selenization occurred uniformly across the substrate. The quantitative EDS spectrum and table (Fig. 2d) indicate an approximate Ni:Se atomic ratio close to stoichiometric nickel selenides, further confirming successful chemical conversion of Ni into $NiSe_2/Ni_3Se_2$ phases. Importantly, no significant segregation of elemental Se was detected in NS-160, unlike the higher-temperature samples where Se redeposition was suggested by XRD (Fig. 1). The elemental mapping below Fig. 2(d) additionally verifies the uniform spatial distribution of Ni and Se, without noticeable clustering or phase separation. This homogeneous composition is critical for stable catalytic performance, as it ensures consistent electronic conductivity and efficient charge transfer pathways across the entire electrode surface.

The oxygen evolution reaction (OER) performance of the nickel selenide electrodes synthesized at different hydrothermal temperatures was evaluated by LSV and Tafel slope analysis (Fig. 3). A clear dependence on synthesis temperature was observed. When the current density was normalized to 100 $mA \cdot cm^{-2}$, the NS-160 electrode required the lowest overpotential (η_{100}) among all samples. This result highlights the excellent intrinsic activity and rapid charge transfer kinetics of NS-160. By contrast, NS-120 and NS-140 exhibited much higher overpotentials at the same current density, consistent with their incomplete crystallization and limited electrochemically active surface areas. At elevated synthesis temperatures (180 and 200°C), the overpotentials decreased relative to low-temperature samples, but they were still higher than that of NS-160, suggesting that excessive crystal growth or partial Se redeposition at high temperature reduces the effective exposure of active sites. The Tafel slope analysis further confirms these trends. NS-160 showed the smallest slope, indicative of faster reaction kinetics and more favorable OER pathways, whereas NS-120 and NS-140 displayed significantly higher slopes, reflecting sluggish kinetics [12]. NS-180 and NS-200 showed moderate improvements compared to low-temperature samples, but still inferior to NS-160. Taken together, these results demonstrate that hydrothermal synthesis at 160°C yields a nickel selenide electrode with the most efficient catalytic properties. The combination of lower overpotential at high current density (100 $mA \cdot cm^{-2}$) and the smallest Tafel slope underscores that NS-160 provides the best balance of crystallinity, conductivity, and accessible active sites, which accounts for its superior OER performance compared to the other samples.

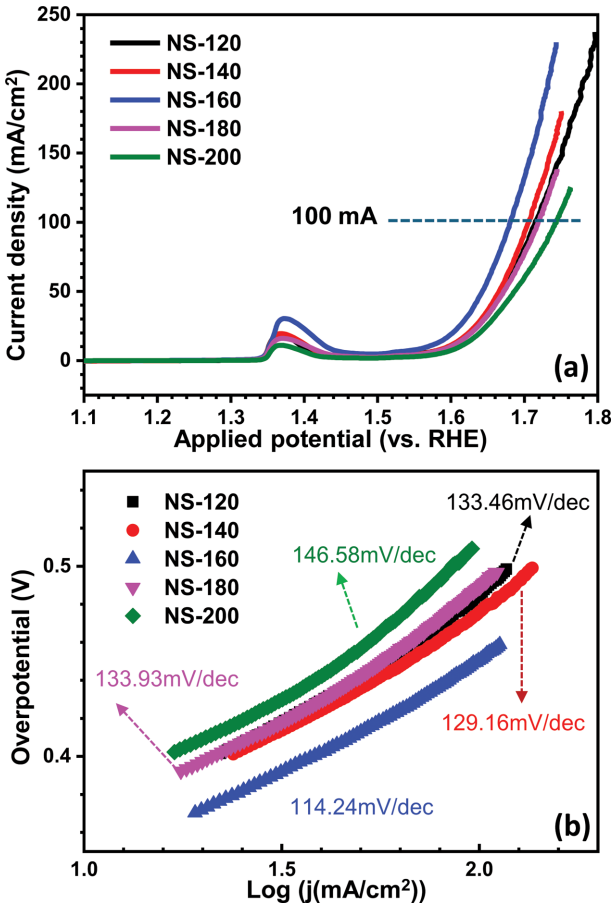

Fig. 3. (a) LSV curves and (b) Tafel slopes of the NS-120, NS-140, NS-160, NS-180 and NS-200 samples.

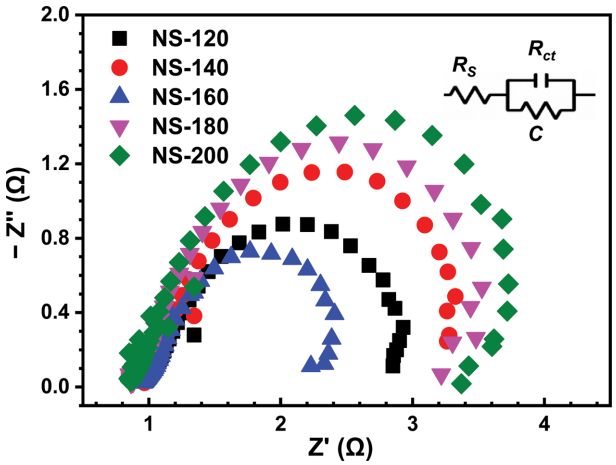

Fig. 4. Nyquist plots of the NS-120, NS-140, NS-160, NS-180 and NS-200 samples.

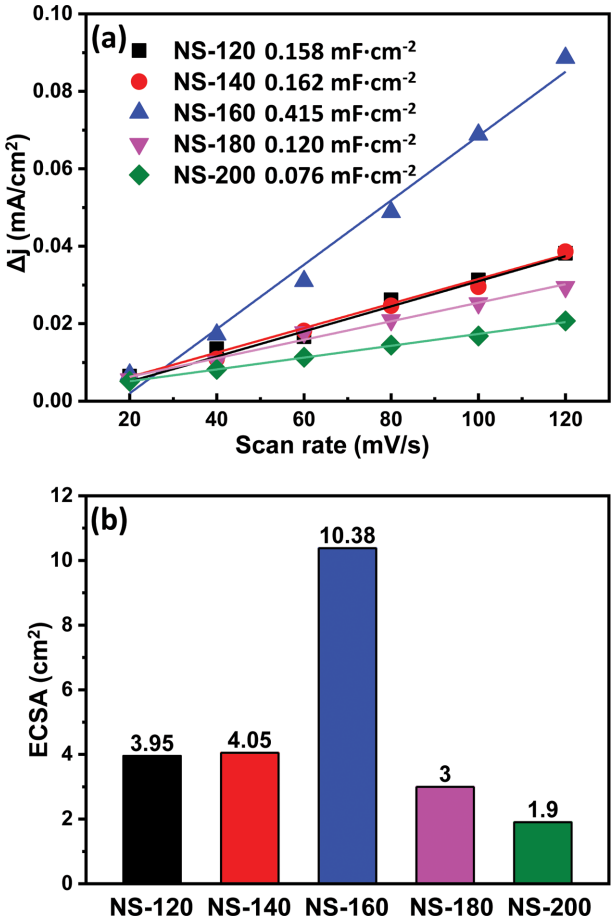

Fig. 5. (a) C_{dl} and (b) ECSA of the NS-120, NS-140, NS-160, NS-180 and NS-200 samples.

The charge transfer characteristics of the nickel selenide electrodes were further investigated by electrochemical impedance spectroscopy (EIS), and the Nyquist plots are shown in Fig. 4. All samples display a typical semicircular arc in the high-to-medium frequency region, corresponding to the charge-transfer resistance (R_{ct}) at the electrode/electrolyte interface, followed by a straight line in the low-frequency region, which is associated with ion diffusion processes [13]. Among the samples, the NS-160 electrode exhibits the smallest semicircle diameter, indicating the lowest R_{ct} value and thus the most efficient electron transfer during the OER process. This implies that the optimized crystalline structure and uniform Ni-Se distribution achieved at 160°C provide highly conductive pathways and abundant active sites that facilitate charge transport. By contrast, the NS-120 and NS-140 electrodes show much larger semicircles, reflecting sluggish interfacial charge transfer due to poor crystallinity and incomplete selenization at lower hydrothermal temperatures. Although the NS-180 and NS-200 electrodes present smaller R_{ct} than the low-temperature samples, their resistance values remain higher than that of NS-160. This can be ascribed to thicker selenide layers or partial Se redeposition at higher temperatures, which increase charge-transfer barriers and limit accessibility of catalytic sites.

The capacitive behavior and accessible active surface area of the nickel selenide electrodes were evaluated through double-layer capacitance (C_{dl}) and electrochemically active surface area (ECSA) analysis, as shown in Fig. 5. In general, C_{dl} provides a measure of the non-faradaic charging current in the double-layer region, which is directly proportional to the number of exposed electroactive sites [14]. ECSA, estimated from C_{dl} values using a standard capacitance constant, reflects the intrinsic surface area available for electrocatalytic reactions. Among all the tested samples, the NS-160 electrode exhibits the highest C_{dl} value (Fig. 5a) and the largest ECSA (Fig. 5b). This clearly indicates that hydrothermal treatment at 160°C produces a nanostructured surface that maximizes the exposure of active sites, thereby facilitating more efficient OER catalysis. These findings are consistent with the FE-SEM observations (Fig. 2), where NS-160 revealed uniformly distributed nanosheet-like features with high surface roughness, which favor increased electrolyte-electrode interaction. In comparison, the NS-120 and NS-140 electrodes show much smaller C_{dl} and ECSA values, reflecting insufficiently developed surface structures due to incomplete selenization at low synthesis temperatures. On the other hand, NS-180 and NS-200 exhibit moderately high C_{dl} and ECSA, but their values remain lower than those of NS-160. This reduction can be attributed to excessive crystal growth or selenium redeposition at higher hydrother-

mal temperatures, which decreases the number of accessible surface sites despite higher bulk crystallinity.

Taken together, the highest C_{dl} and ECSA of NS-160 confirm that it possesses the greatest density of catalytically active sites, which directly correlates with its lowest overpotential (Fig. 3) and smallest charge-transfer resistance (Fig. 4). These results provide further evidence that hydrothermal synthesis at 160°C yields the most favorable balance of crystallinity, morphology, and surface accessibility for achieving superior OER performance.

4. Summary

In summary, nickel selenide electrocatalysts were successfully synthesized on Ni foam via a facile hydrothermal route using elemental Se powder and hydrazine. By systematically varying the synthesis temperature from 120 to 200°C, the relationship between phase evolution, morphology, and OER performance was elucidated. XRD analysis revealed that well-crystallized $NiSe_2$/Ni_3Se_2 phases formed most effectively at 160°C, while FE-SEM and EDS confirmed a uniform nanosheet-like structure and homogeneous Ni-Se distribution. Electrochemical evaluation demonstrated that the NS-160 electrode exhibited the best catalytic activity, requiring the lowest overpotential to reach 100 $mA \cdot cm^{-2}$, together with the smallest Tafel slope, the lowest charge-transfer resistance, and the highest C_{dl} and ECSA values. These results clearly indicate that an optimized balance between crystallinity and morphology at 160°C maximizes active site exposure and facilitates efficient charge transfer, leading to superior OER performance. This study provides useful insights into the rational design of nickel selenide-based self-supported electrodes and offers a cost-effective strategy for developing efficient electrocatalysts for alkaline water electrolysis.

Acknowledgement

This work was supported by the National Research Foundation of Korea (NRF) grant funded by the Korean Government (MSIT) (RS-2024-00342443).

References

[1] M. Chatenet, B.G. Pollet, D.R. Dekel, F. Dionigi, J. Deseure, P. Millet, R.D. Braatz, M.Z. Bazant, M. Eikerling, I. Staffell, P. Balcombe, Y. Shao-Horn and H. Schäfer, "Water electrolysis: from textbook knowledge to the latest scientific strategies and industrial developments", Chem. Soc. Rev. 51 (2022) 4583.

[2] H. Over, "Fundamental studies of planar single-crystalline oxide model electrodes (RuO_2, IrO_2) for acidic water splitting", ACS Catal. 11 (2021) 8848.

[3] Z. Ma, Y. Zhang, S. Liu, W. Xu, L. Wu, Y. Hsieh, P. Liu, Y. Zhu, K. Sasaki, J.N. Renner, K.E. Ayers and R.R. Adzic, "Reaction mechanism for oxygen evolution on RuO_2, IrO_2, and RuO_2@IrO_2 core-shell nanocatalysts", J. Electroanal. Chem. 819 (2018) 296.

[4] P.M. Bodhankar, P.B. Sarawade, G. Singh, A. Vinu and D.S. Dhawale, "Recent advances in highly active nanostructured NiFe LDH catalyst for electrochemical water splitting", J. Mater. Chem. A 9 (2021) 3180.

[5] D. Tyndall, M.J. Craig, L. Gannon, C. McGuinness, N. McEvoy, A. Roy, M. García-Melchor, M.P. Browne and V. Nicolosi, "Demonstrating the source of inherent instability in NiFe LDH-based OER electrocatalysts", J. Mater. Chem. A 11 (2023) 4067.

[6] S. Anantharaj and S. Noda, "Nickel selenides as pre-catalysts for electrochemical oxygen evolution reaction: A review", Int. J. Hydrog. Energy 45 (2020) 15763.

[7] A.T. Swesi, J. Masud and M. Nath, "Nickel selenide as a high-efficiency catalyst for oxygen evolution reaction", Energy Environ. Sci. 9 (2016) 1771.

[8] A. Sivanantham and S. Shanmugam, "Nickel selenide supported on nickel foam as an efficient and durable non-precious electrocatalyst for the alkaline water electrolysis", Appl. Catal. B-Environ. 203 (2017) 485.

[9] C. Yang, Y. Lu, W. Duan, Z. Kong, Z. Huang, T. Yang, Y. Zou, R. Chen and S. Wan, "Recent progress and prospective of nickel selenide-based electrocatalysts for water splitting", Energy Fuels 35 (2021) 14283.

[10] K. Xu, H. Ding, H. Lv, S. Tao, P. Chen, X. Wu, W. Chu, C. Wu and Y. Xie, "Understanding structure-dependent catalytic performance of nickel selenides for electrochemical water oxidation", ACS Catal. 7 (2017) 310.

[11] D.H. Yoo, T.K. An, Y.S. Jang and J.H. Ryu, "Synthesis of rGO/CoNi LDH composite and enhancement of oxygen evolution reaction", J. Kor. Cryst. Growth Cryst. Technol. 35 (2025) 21.

[12] J. Zhang, H.B. Yang, D. Zhou and B. Liu, "Adsorption Energy in Oxygen Electrocatalysis", Chem. Rev. 122 (2022) 17028.

[13] N. Zhou, Q. Wang, J. Zhu, N. Zhou, X. Chai, M. Li, Z. Pei, K. Hu, Z. Huang and B. Chen, "Interface engineering of Ni_3S_2 coupled NiFe-LDH heterostructure enables superior overall water splitting", Mater. Today Chem. 43 (2025) 102510.

[14] S.S. Jeon, P.W. Kang, M. Klingenhof, H. Lee, F. Dionigi and P. Strasser, "Active surface area and intrinsic catalytic oxygen evolution reactivity of NiFe LDH at reactive electrode potentials using capacitances", ACS Catal. 13 (2023) 1186.